Proceedings of ASME Turbo Expo Turbine Technical Conference
IGTI 2011
June 6-10, 2011, Vancouver, Canada

GT2011-46356

TIP CLEARANCE INVESTIGATION OF A DUCTED FAN USED IN VTOL UAVS

PART 1: BASELINE EXPERIMENTS AND COMPUTATIONAL VALIDATION

Ali Akturk[*]
Turbomachinery Aero-heat Transfer Laboratory
Department Aerospace Engineering
The Pennsylvania State University
University Park, Pennsylvania 16802
Email: aua162@psu.edu

Cengiz Camci [†]
Turbomachinery Aero-heat Transfer Laboratory
Department Aerospace Engineering
The Pennsylvania State University
University Park, Pennsylvania 16802
Email: cxc11@psu.edu

ABSTRACT

Ducted fans that are popular choices in vertical take-off and landing (VTOL) unmanned aerial vehicles (UAV) offer a higher static thrust/power ratio for a given diameter than open propellers. Although ducted fans provide high performance in many VTOL applications, there are still unresolved problems associated with these systems. Fan rotor tip leakage flow is a significant source of aerodynamic loss for ducted fan VTOL UAVs and adversely affects the general aerodynamic performance of these vehicles. The present study utilized experimental and computational techniques in a 22" diameter ducted fan test system that has been custom designed and manufactured. Experimental investigation consisted of total pressure measurements using Kiel total pressure probes and real time six-component force and torque measurements. The computational technique used in this study included a 3D Reynolds-Averaged Navier Stokes (RANS) based CFD model of the ducted fan test system. RANS simulations of the flow around rotor blades and duct geometry in the rotating frame of reference provided a comprehensive description of the tip leakage and passage flow. The experimental and computational analysis performed for various tip clearances were utilized in understanding the effect of the tip leakage flow on aerodynamic performance of ducted fans used in VTOL UAVs. The aerodynamic measurements and results of the RANS simulations showed good agreement especially near the tip region.

NOMENCLATURE

c Chord length
C_p Static pressure coefficient
C_{pt} Total pressure coefficient, $C_{pt} = \frac{P_{te}-P_{ti}}{\frac{1}{2}\rho U_m^2}$
C_P Power coefficient, $C_P = \frac{\text{Power}}{\rho\omega^3 D^5}$
C_T Thrust coefficient, $C_T = \frac{\text{Thrust}}{\rho\omega^2 D^4}$
D Shroud (casing) inner diameter (m)
h Blade height
IC Internal combustion
p Static pressure
PS Pressure side
R Ideal gas constant,(for air $R = 287\ \frac{J}{Kg\cdot K}$)
RANS Reynolds-Averaged Navier Stokes
SS Suction side
t Effective tip clearance in inches
t/h Relative tip clearance wrt blade height
UAV Uninhabited Aerial Vehicles
$VTOL$ Vertical Take-Off and Landing
y^+ Non-dimensional wall distance

INTRODUCTION

The flow field resulting from the region between the stationary duct and rotor tip of a ducted fan is complicated because of the interaction of the tip leakage flow, annulus wall boundary layer and rotor wake. The inherent pressure difference be-

[*]Postdoctoral Research Fellow
[†]Professor of Aerospace Engineering, corresponding author

tween the pressure side and suction side of blade tip generates a tip leakage flow. The leakage flow also rolls into a highly three dimensional tip leakage vortex with significantly turbulent and unsteady flow features in each passage. The tip leakage vortex is a complex flow phenomenon that is one of the dominant mechanisms of noise generation by unsteady interactions in a turbomachinery system. It is a significant energy loss mechanism in the ducted fans .

This paper describes investigations on tip clearance flow for ducted fans. The common design principle of ducted fan is to ensure the tip clearance as small as possible to reduce tip leakage losses and improve aerodynamic performance. Indeed this is still the case for ducted fans used in VTOL UAVs, the clearance is unavoidably kept large because of the operating conditions. There are many small diameter VTOL UAV systems using Internal Combustion (IC) engines as power source. The IC engine driven systems suffer from strong mechanical vibrations.

There has been a limited number of studies about three dimensional flow structure of leakage vortex in axial flow fans and compressors, in open literature [1–5]. Inoue and Kuroumaru et al. [6] made detailed flow measurements before and behind an axial flow rotor with different tip clearances. In their study, they investigated the clearance effect on the behavior of tip leakage flow. Furukawa and Inoue et al. [7] also investigated breakdown of tip leakage vortex in a low speed axial flow compressor. Reducing tip leakage mass flow rate in general improves the aerodynamic performance of axial flow fans and compressors. Implementation of treatments in the non-rotating part over the blade tip is also an efficient way of tip leakage flow reduction. References [8] and [9] investigate different casing treatments for axial flow compressors.

The wake developed from an axial flow fan has a strong influence on the system performance. It is a significant source of aerodynamic loss and affects the efficiency and vibration characteristics. References [10–12] deal with extensive investigations of the wake flow features such as mean velocities, turbulence and decay characteristics on turbomachinery performance. The wake flow system is likely to interact with the complex flow system originating in the tip gap region.

Few authors investigated the influence of large tip clearances in turbomachinery components. Large tip clearances are not typically found within axial flow fans and compressors designed for aero-engines. Williams et al. [13] investigated large tip clearances in the high pressure compressor stages used in industrial gas turbines. They have carried out an comprehensive study on two different compressor cascades. They used five-hole pressure probe measurements at upstream and downstream of the cascades. The authors have shown that tip leakage flow is more important parameter influencing the rotor exit flow pattern than blade shape.

Ducted fan VTOL UAVs need to fly in a broad range of atmospheric conditions because of their complicated missions. Their performance is highly affected from large tip clearance. There has been only a few studies about ducted fan aerodynamic and aeromechanic performance. Pereira performed an experimental study on the effects of various shroud profile shapes on the performance of MAV-scale shrouded rotors [14]. Seventeen ducted fan models with a nominal rotor diameter of 16 cm (6.3 in) and various values of diffuser expansion angle, diffuser length, inlet lip radius and blade tip clearance were tested at various rotor collective angles. Tests performed for open rotor and a single shrouded-rotor model at a single collective in translational flight, at angles of attack from 0^o (axial flow) to 90^o (edgewise flow), and at various advance ratios are reported.

Martin and Tung [15] tested a ducted fan V/STOL UAV with a 10-inch diameter rotor. They measured aerodynamic loads on the vehicle for different angles of attack (from 0^o to 110^o) in hover and different crosswind velocities. Both models were tested with fixed-pitch propellers of varying diameters, to test tip clearances from 1% to 4% (based on rotor tip radius). They also included hot-wire velocity surveys at inner and outer surface of the duct and across the downstream wake emphasizing the effect of tip gap on the thrust force produced. In addition, their study showed the effect of leading edge radius of the duct on the stall performance and stability of the vehicle. They have shown that the thrust of the system is decreasing with increasing tip gap height. Their results also showed that for lower rotational speeds open rotor thrust was higher than ducted fan thrust. They explained this by pointing out the increase in viscous losses inside the duct for low rotational speed operations.

Martin and Boxwell [16] tested two ducted fan models that were designed to effectively eliminate the tip leakage. Both models were derived from the baseline (10-inch inner-diameter shroud) which is explained in their previous study [15]. In their fist design, they have created a notch and fit the propeller inside the notch. In their second design, a rearward-facing step was cut into the inner shroud. The computational analysis resulted in an increase in inlet lip suction and an increase in performance. However, the experimental thrust and power measurements, showed no difference in performance of these designs when compared to their baseline duct.

In the present investigation, experimental and computational methods were used to investigate the effect of tip clearance flow on ducted fan aerodynamic performance. A 22" ducted fan test system was designed and manufactured for experimental investigations. Total pressure measurements were performed at the downstream of the fan rotor using a traversing Kiel probe. Inlet total pressure and axial velocity were also monitored at the midspan location. Aeromechanic performance of the ducted fan was measured using a six axis force and moment transducer. Beside the experimental measurements, computational analyses were carried out for the ducted fan system in hover condition. The main goal of this paper is to investigate the large tip clearance effect in ducted fans for VTOL UAV applications. The ex-

perimental data obtained were also used to validate the computational method outlined in this paper. The computational method is also going to be used in development of tip treatments. The results from an investigation dealing with the new tip treatments designed and analyzed using this validated computational approach are presented in an accompanying paper by Akturk and Camci [17].

EXPERIMENTAL METHOD

Facility Description

The 22" diameter ducted fan test system with a realistic disk loading found in most present day VTOL UAV systems is shown in Figure 1. The main components in the flow path of this facility are listed as follows:

- ◇ Inlet lip section (replaceable)
- ◇ Eight-bladed axial fan rotor
- ◇ 20 Hp DC brushless electric motor
- ◇ Diffuser section
- ◇ Six component force and torque measurement system

Figure 1 shows the main components of instrumentation integrated into this research facility. Test system is equipped with a radially traversing Kiel total pressure probe downstream of the axial flow fan rotor, a stationary total pressure probe at the inlet of the duct, an optical once-per-rev sensor, a pitot probe for velocity measurements at the duct inlet and an ATI six component force and torque measurement transducer. The system also has a number of thermocouples and various electrical monitoring systems for electrical safety.

Ducted Fan Model

The ducted fan used in current experiments is composed of a shroud, axial flow fan, inlet lip and exit diffuser. The shroud is manufactured from thermoplastic material and has an inner radius of 11.15 inches. It is connected to the main support using four 12.7 mm (0.5") diameter stainless steel threaded circular rods. Threaded rods connect shroud to the central support system. The center support holds the ducted fan so that the fan rotor is about three rotor diameters away from the ground which guarantees measurements are free from ground effect.

The 22" diameter ducted fan was designed to provide a realistic disk loading typical of VTOL UAVs. The 22" diameter ducted fan shown in Figure 1 provides 828.3 Pa (17.3 lb/ft^2) disk loading under nominal operating conditions (3500 rpm).

The geometry of the duct inlet lip shape can be described by two distinct characteristics: wall thickness (t_w) and leading edge radius of curvature (ρ_{LE}). Wall thickness is the maximum thickness of the airfoil shape used to make up the wall of the duct, and the leading edge radius of curvature describes the roundness of the duct lip. The inlet lip shape was designed to have a relatively

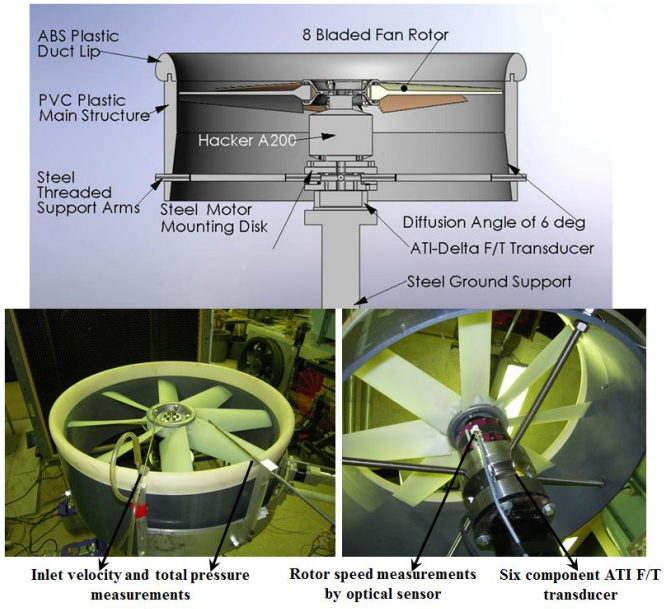

FIGURE 1: Schematic and Instrumentation of the 22" diam. ducted fan system

small leading edge radius. The reduced leading edge radius usually allows the adverse pressure gradient to change gradually inside the lip. Changing pressure gradient gradually helps reducing inlet lip separations inside the duct lip especially under edgewise flight conditions. The t_w and ρ_{LE} used for this ducted fan were 11 % and 3.61 % of the duct chord respectively. The diffuser section was designed to augment the thrust generated by the ducted fan. Diffuser half angle at the exit is six degrees. The axial length of the diffuser is about 117.85 mm (4.64").

Fan Rotor The eight-bladed fan rotor was designed and manufactured by Multi-Wing International. The fan blades were designed for high flow coefficient. The rotor blades were manufactured from a high quality thermoplastic (Glass Reinforced Polyamide). Rotor blades are attached to a custom designed aluminum hub. This specific hub system allows a quick replacement of the rotor assembly in this research facility. Figure 2 shows blade profiles at various radial stations. Table 1 presents fan rotor and blade section geometrical properties.

A 20 Hp A200-6 brushless electric motor (Hacker) directly drives axial flow fan rotor in the 22" diameter ducted fan research facility. The electric motor was controlled by an electronic speed controller (MasterSPIN-220-OPTO ESC). Electrical power for the motor was supplied by 4 deep cycle lead acid batteries connected in series. Due to high torque characteristic of the electric motor, the electric current and temperature of the motor was continuously monitored for operational safety.

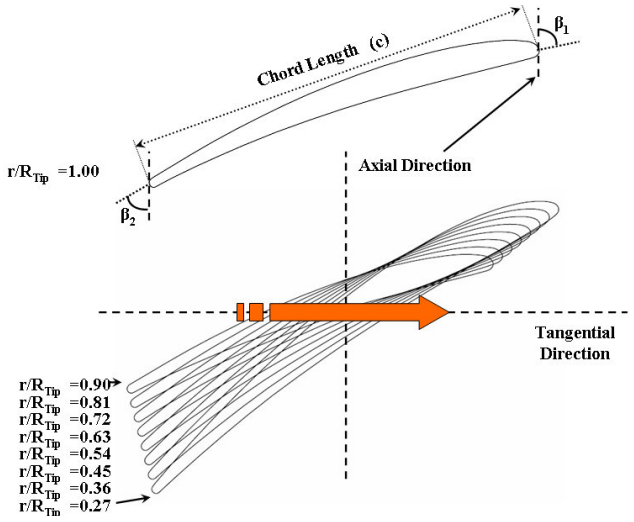

FIGURE 2: Blade profiles at various radial stations

Rotor hub radius	63.5 mm (2.5 in) (r/R_{tip} =0.227)
Rotor tip radius	279.4 mm (11.0 in)(r/R_{tip} =1.000) for 1.71% tip clearance
Rotor pitch angle	55^o
Number of blades	8
Max thickness at rotor tip	5.15 mm (0.216 in)

Blade section properties

radius (mm)	r/R_{tip}	β_1	β_2	chord (mm)
76.2	0.27	71.87	40.77	84.3
101.6	0.36	72.81	43.50	81.5
127.0	0.45	76.56	46.30	78.8
152.4	0.55	78.37	49.94	75.9
177.8	0.64	79.52	52.13	73.1
203.2	0.73	80.31	53.64	70.6
228.6	0.82	82.87	56.51	68.1
254.0	0.91	84.00	58.39	65.8
279.4	1.00	85.21	60.92	63.8

TABLE 1: Fan rotor geometric and blade section properties

INSTRUMENTATION OF THE 22" DUCTED FAN

Rotor Exit Total Pressure Measurements Fan rotor exit total pressure measurements were performed by using a Kiel total pressure probe. The Kiel total pressure probe having a 5 mm diameter total head was traversed in radial direction using a precision linear traverse mechanism. The total pressure probe was always located 45.72 mm downstream of the fan rotor exit plane at 50% blade span (mid-span).

The Kiel probe manufactured by United Sensors Corporation is relatively insensitive to incoming angle of the flow (yaw angle). The range of insensitivity to misalignment for this probe is about $\pm 52^o$ to see a more than 1 % deviation from the inlet dynamic head [18]. The accurate orientation of the Kiel probe in a problem where yaw angle varies dramatically near the tip section of the blade is extremely challenging. A computational fluid dynamics approach was used to properly align the probe with respect to axial direction. Preliminary computations of rotor exit flow field were performed using Ansys CFX RANS solver. Details of this computational analysis can be found in the following sections. Figure 3 shows computed distribution of absolute flow yaw angle at the fan rotor exit where Kiel probe was located. Figure 3 shows that the absolute yaw angle is not changing significantly near the mid-span for radial stations $0.38 \leq r/R_{tip} \leq 0.90$. The average yaw angle obtained on these stations is 18^o which is shown by blue straight line in Figure 3. The Kiel probe was aligned at this average angle at these locations. Although flow angles varied by the effect of the three dimensional features such as passage vortex and hub seperation near the hub region, the Kiel probe was assumed to capture flow field because of its $\pm 52^o$ yaw angle tolerance. Because the tip region, where $r/R_{tip} \geq 0.90$, was affected by the tip leakage vortex, tangential velocity component changed due to this vortical field and yaw angle increased abruptly in this region. The Kiel probe was manually aligned by the "*averaged*" computed absolute flow yaw angles in this region. The probe was aligned at 62^o angle around the tip region.

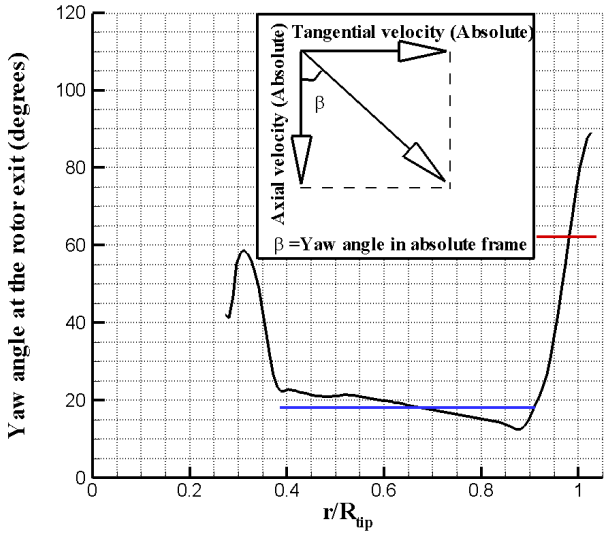

FIGURE 3: Yaw angle in absolute frame calculated from initial computations

The Kiel total pressure head was connected to a Validyne DP 15 variable reluctance pressure transducer that was referenced to

atmospheric pressure. The output of the transducer directly connected to Validyne CD 15 carrier demodulator that gives a linearized analog output in the range of $\pm 10V$. The calibration of the pressure transducer required applying a known pressure to the transducer and recording the associated voltage. The relationship between the pressure and voltage was linear because an external demodulator linearization was employed. The Validyne carrier demodulator was connected to a 12bit data acquisition board (MCC 1208FS). Analog signals were transfered to computer and analyzed by Labview data acquisition software, custom developed for the current research effort. The 5 second data acquisition time was selected as sampling time for the experiments so the Kiel probe pneumatic output reached steady state and a statistically stable averaged total pressure reading was recorded.

The inlet conditions for ducted fan system were also monitored using a Kiel total pressure probe and a conventional pitot probe. Both probes were mounted over the duct lip at mid-span of fan rotor. The conventional Pitot probe with a static and total hole measured the magnitude of the inlet axial velocity at mid-span. Total pressure at duct inlet was measured using the same procedure outlined for the rotor exit total pressure probe without "*nulling*". Data acquisition time for this probe was also set to 5 seconds. Pitot probe was used to obtain duct inlet velocity. Both probes were aligned with the axial flow direction, since the flow at the inlet of the ducted fan where flow was free from tangential and radial components.

Six Component Force and Moment Measurement

Ducted fan aerodynamic research performed in this study requires high accuracy force and moment measurements. The 22" diameter fan is equipped with an ATI-Delta six component force and torque transducer. The ATI Multi-Axis Force/-Torque Sensor system measures all six components of the force and moment. Three components of force and three components of moments are measured. It consists of a transducer assembly, a shielded high-flex cable, and a 16-bit data acquisition system and a F/T controller. A software system provided by ATI was used to convert the transducer readings into force and torque output in engineering units using the calibration data provided. The thrust and moment transducer is factory calibrated with known forces and moments. The accuracy of the transducer was ± 0.033N for forces in x direction, ± 0.033N for forces in y direction,± 0.099N for forces in z direction, ± 0.003N.m for moments in x direction,± 0.003N.m for moments in y direction and ± 0.003N.m for moments in z direction.

COMPUTATIONAL METHOD

A three dimensional computational method is used for analyzing viscous and turbulent flow field around and inside the ducted fan and especially complicated flow field near the fan rotor tip for hover condition.

A simulation of the incompressible mean flow field around the ducted fan was performed using the general purpose fluid dynamics solver Ansys-CFX. The specific computational system solves the Reynolds-Averaged Navier-Stokes (RANS) equations using an element based finite volume method in the ducted fan rotor and around the ducted fan driven VTOL UAV. The mass, momentum and energy equations are simultaneously solved over an unstructured finite volume based mesh system.

The k-ω based shear stress transport model is used in our computations [19]. This model accounts for the transport of the turbulent shear stress and gives accurate predictions of the flow separation under adverse pressure gradient.

Computational Domains and Boundary Conditions

The computational analysis for ducted fan aerodynamic investigation in hover was performed on three separate computational domains, that are connected. The stationary inlet and outlet regions and rotating fan rotor region are shown in Figure 5. Inlet region includes an inlet lip surface that was considered as a solid wall with no-slip condition. Atmospheric static pressure was prescribed on the top surface. On the side surface, an opening type boundary condition was assumed. An opening boundary condition allows the fluid to cross the boundary surface in either direction. For example, all of the fluid might flow into the domain at the opening, or all of the fluid might flow out of the domain, or a combination of the two might occur. An opening boundary condition might be used where it is known that the fluid flows in both directions (any direction) across the boundary.

The outlet region includes the outer duct surface, circular rods, rotor hub surface and support structure underneath of the system that is considered as solid walls with no-slip condition. Bottom surface is also treated with no-slip boundary condition. On the side surface, an opening boundary condition is assumed.

The rotating region includes fan blades, rotor hub region and shroud surface where rotating fluid motion is simulated by adding source terms. Additional sources of momentum are required to account for the effects of the Coriolis force and the centrifugal force. Counter rotating wall velocities are assigned at the shroud surface.

Stationary and rotating regions were sub-sectional by periodic surfaces. By the help of periodicity, speed of numerical simulations was increased. The stationary surfaces were divided into 4 segments and rotating region was divided into 8 periodic segments. Only one of these segments for each region was used in numerical calculations. Difference in pitch angles of the frames is taken into account in interfaces that are connecting rotating and stationary surfaces. A stage type interface model was used.

Stage Interface When one side is in a stationary frame and the other side is in rotating frame of reference, an interface

should be used for connection. "Stage" type interface model is used in calculations for modeling frame change. The stage model performs a circumferential averaging of the fluxes on the interface. This model allows steady state predictions to be obtained for turbomachinery components. The stage averaging at the frame change interface introduce one-time mixing loss. This loss is equivalent to assuming that the physical mixing supplied by the relative motion between components. Between stationary frames an interface provides general connection between two stationary domains. General grid interface (GGI) is used for mesh connections between interfaces.

Grid Refinement Study

A grid independence study is performed to show that the computational results are not dependent on the computational mesh and the resolution of the mesh is adequate to capture the significant flow characteristics. The grid independence is evaluated by comparing the computational solutions from 3 different mesh sizes, comprising a coarse mesh with 3,000,000 tetrahedral cells, medium mesh with 4,750,000 cells and 6,000,000 cells. The static pressure distribution around the midspan blade profile at the radial station $r = 0.90$ for baseline fan rotor is plotted in Figure 4 for three different grid densities. The profile suggests that the computational results are grid independent when the 4,700,000 cells are exceeded. Therefore, the medium mesh is used for all predictions in this chapter. Figure 5 illustrates a view from medium size computational mesh near the inlet lip region and rotor tip. The unstructured tetrahedral cells are used for computations. Regions near the solid surfaces are meshed with prisms for generating a better viscous boundary layer grid. Non-dimensional wall distance (y^+) less than 2 is achieved near the shroud and hub region. Region between solid shroud and rotating blade tips is filled with prism layers.

EXPERIMENTAL RESULTS

Force and Torque Measurements

The most significant force and moment component that is measured for the ducted fan system in hover condition is thrust and rotor torque which are F_z and T_z as shown in Figure 1. Other components may become significant, when the ducted fan is operated in non-symmetric inlet conditions such as forward flight operation. Although three components of forces and moments were measured, only the thrust and torque of the ducted fan will be presented throughout this paper since all of the measurements are performed in hover condition. The thrust and torque measurements were obtained at hover condition for a number of rotor speeds. Thrust measurements are normalized as thrust coefficient, defined as;

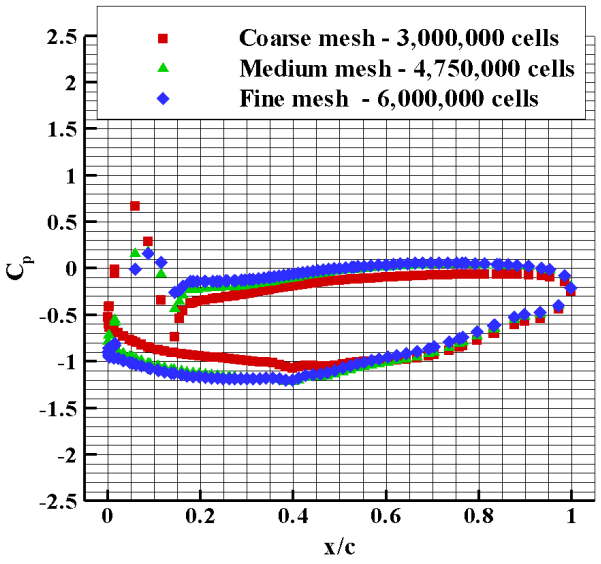

FIGURE 4: Grid independence study

$$C_T = \frac{Thrust}{\rho\Omega^2 D^4} \quad \text{where} \quad \rho = \frac{P_a}{RT_a} \tag{1}$$

Torque measurements were essential in calculating required power using the relationship between torque and power ($Power = Torque \times \Omega$). The measured power was normalized as a power coefficient.

$$C_P = \frac{Power}{\rho\Omega^3 D^5} \quad \text{where} \quad \rho = \frac{P_a}{RT_a} \tag{2}$$

The figure of merit was calculated as a measure of hover efficiency for the ducted fan. The figure of merit was defined as;

$$\text{Figure of Merit (FM)} = \frac{C_T^{3/2}}{\sqrt{2}C_P} \tag{3}$$

Figure 6 shows calculated thrust coefficient for the 22" ducted fan with baseline fan rotors at various rotational speeds. The ducted fan thrust was measured for various tip clearances. The fan rotor only thrust was also measured. The fan rotor only thrust was measured by using 10.89" tip diameter fan rotor which is the identical rotor used for 3.04 % tip clearance study. The tip clearances were adjusted by changing the fan rotor diameter as

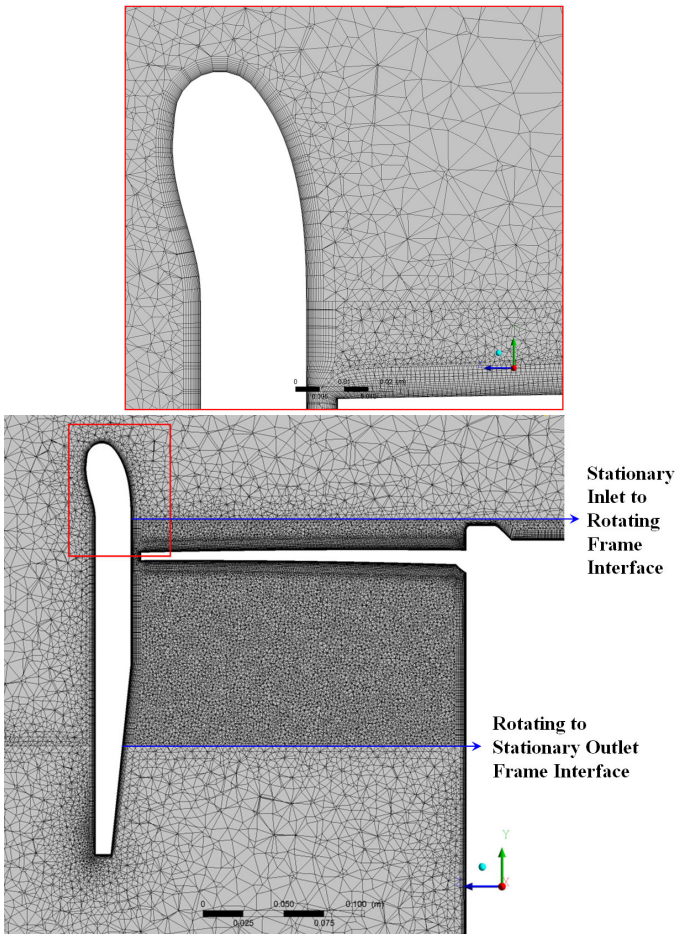

FIGURE 5: Medium size computational mesh used in computations

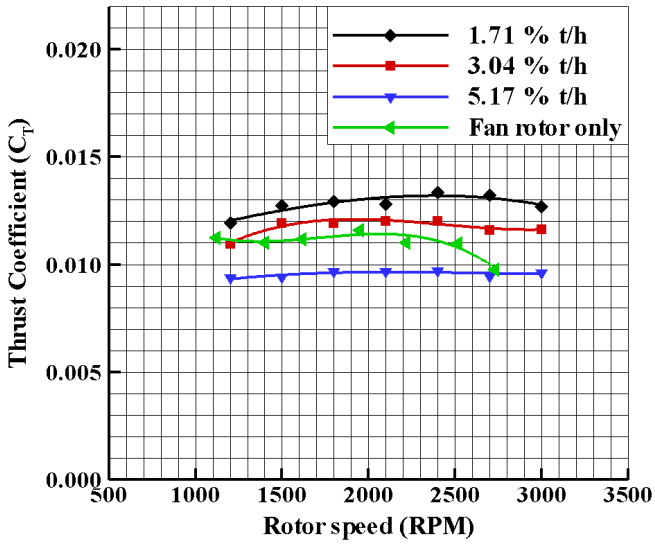

FIGURE 6: Thrust coefficient versus fan rotational speed during hover (baseline rotor)

mentioned previously.

The variable tip clearance study presented in this chapter used custom made rotors with accurately adjusted tip diameters in a shroud system having a constant inner diameter. Using a ducted fan around an open rotor improves the thrust of the system as compared to an open rotor for tip clearances of 3.04 % and 1.71 %. For the tip clearance of 5.17 %, the open rotor provides more thrust. This observation can be explained by the effect of increased viscous losses and tip leakage related losses. The losses generated when the shroud is added to the fan rotor is so high that the additional thrust due to duct lip and shroud is almost eliminated. It should also be noted that decreasing the tip gap height is effective at improving performance of the system and results in augmented thrust generation.

The thrust force generated per supplied power for various baseline configurations is shown in Figure 7. The data is arranged in the form of thrust coefficient C_T versus power coefficient C_P The smallest tip clearance configuration generates the highest thrust per unit of power supplied. Since increasing tip clearance is also increases losses in the system, power demand of the system also increases.

Figure 8 shows another key result of this study. The sensitivity of hover efficiency to increasing tip gap is shown. It should be noted that using a ducted fan configuration also improved hover efficiency by 38 % for the higher rotational speed. Decreasing tip clearance is effective in increasing the hover efficiency. Decreasing tip clearance from 3.04 % to 1.71 % increased hover efficiency of the system by 17.85 % at the higher rotor speed.

Total Pressure Measurements at Rotor Exit

The aerodynamic performance of the ducted fan was quantified by rotor exit total pressure measurements at hover condition for 2400 rpm. The results are presented with non-dimensional total pressure coefficient which is defined as;

$$C_{pt} = \frac{P_{te} - P_{ti}}{\frac{1}{2}\rho U_m^2} \text{ where } \rho = \frac{P_a}{RT_a} \tag{4}$$

where U_m is the rotor speed calculated at the mid-span, $U_m = r_m \times \Omega$. Random uncertainty of total pressure coefficient was calculated as ± 0.002 [20, 21].

Figure 9 shows the total pressure coefficient measured a downstream position from rotor hub to shroud. It should be noted

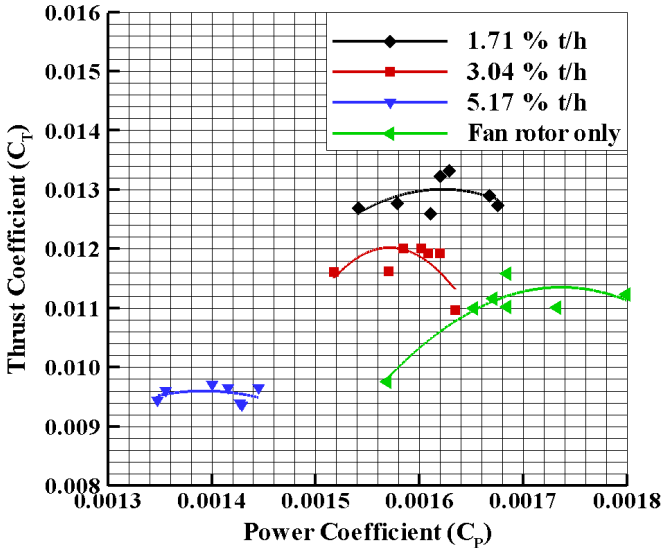

FIGURE 7: Thrust coefficient vs power coefficient for the baseline rotor

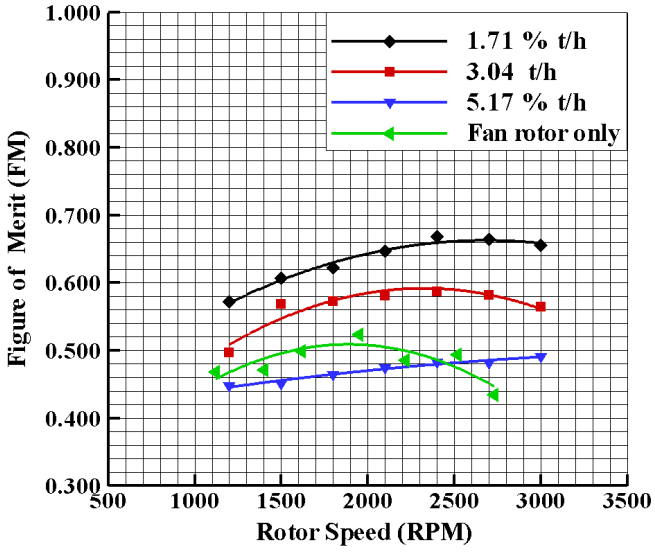

FIGURE 8: Figure of Merit (FM) vs fan rotational speed for the baseline rotor

that there is almost no change in total pressure coefficient by changing the tip clearance for $r/R_{tip} \leq 0.65$. Flow near the rotor hub is not affected by the tip leakage losses. When the tip clearance is 5.17 %, the losses related to the tip leakage vortex are increased at a significant rate, because of the increased tip vortex size.

COMPUTATIONAL RESULTS

Computational Model Validation

Total Pressure at the Rotor Exit Figure 10 shows a comparison of experimental and computational results for 1.71 %, 3.04% and 5.17 % tip clearances. Circumferentially averaged total pressure coefficient at the downstream of the fan rotor is compared to the experimental results. The computational and experimental results show very good agreement in the spanwise distribution except in a limited area near the hub where r/$R_{tip} \leq$ 0.65. The computational results slightly deviate from experimental results near the hub region. That is because of the highly complex low Reynolds number and possibly re-circulatory turbulent flow field near the hub region. Low Reynolds number characteristic of the flow makes this computation highly challenging. Reynolds number based on blade chord is approximately lower than 50,000 at the r/$R_{tip} \leq 0.6$. Low Reynolds number flows are relatively hard to compute using standard turbulent models as they are used in present day computational systems. The overall results show significant re-circulatory flow zones near the hub wall. The highly 3D and possibly unsteady flow zones are driven

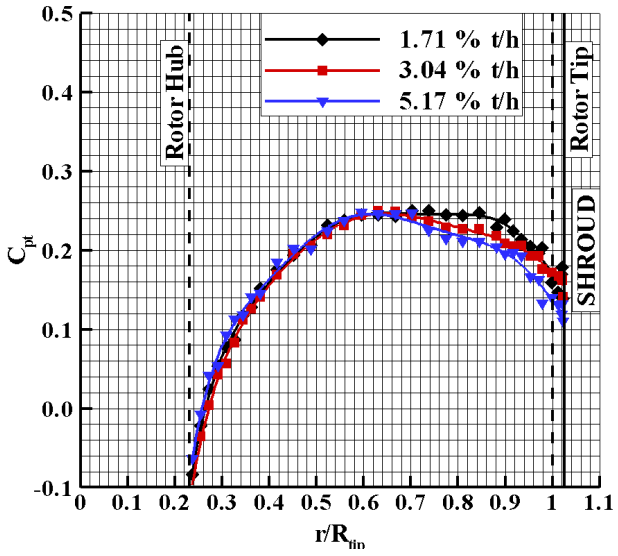

FIGURE 9: Total pressure measured at downstream of the rotor at 2400 rpm for baseline rotor

by the hub inlet (corner) region flows.

Thrust and Power Curves Figure 11 shows the variation of thrust with rotational speed obtained from experiments as well as the computational results for two different tip clear-

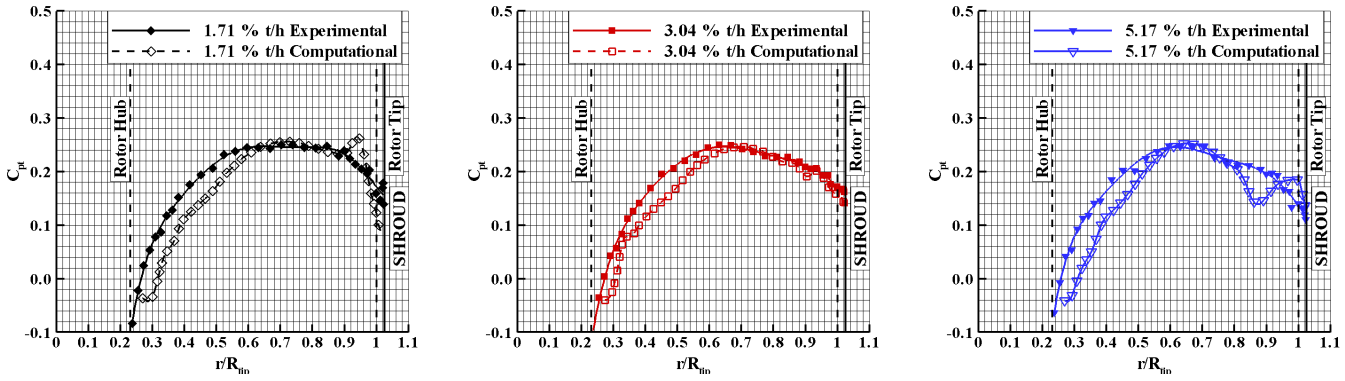

FIGURE 10: Total pressure coefficient comparison for experimental and computational analysis at 2400 rpm for baseline rotor with (a) 1.71 %, (b) 3.04% and (c) 5.17 % tip clearances

ances. Clearly, the computational results agree well with the experimental data for both tip clearances especially for low rotational speeds. The relative error increases for rotor speeds higher than 2400 rpm.

Computed rotor thrust and duct thrust are also shown in Figure 11. As the tip clearance increases, the rotor thrust decreases because of the increased tip leakage flow. Tip leakage flow is quantified by calculating leakage mass flow rate. Leakage mass flow rate is 1.81 % of the mass flow rate of the fan rotor for 1.71% tip clearance. When tip clearance increased to 3.04 %, leakage mass flow rate is also increased to 3.41% of the fan rotor mass flow rate. That increase in leakage mass flow rate increased losses in the main fan flow, and decreased rotor thrust. Although duct thrust was the same for both tip clearances for low rotor speeds, it increased for high rotor speed as tip clearance decreased. The main reason for this improvement in duct thrust is an increase in axial velocity component of the velocity especially for high rotor speeds.

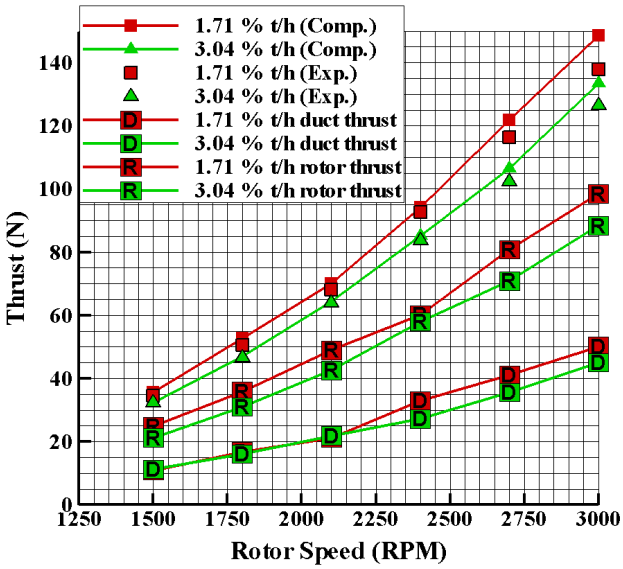

FIGURE 11: Comparison of computed and measured thrust for 1.71 % and 3.04% tip clearance for baseline rotor

Flow Field Analysis

Effect of tip leakage and secondary flows on fan rotor exit performance The flow field between the stationary shroud and rotor tip of a ducted fan is highly complex because of the interaction of the leakage flow, annulus wall boundary layer and rotor wake. Figures 12 and 14 show the streamlines drawn around the rotor blade with 1.71 % and 3.04 % tip clearance respectively. The complex flow features near the tip and mid-span region are visualized at a high spatial resolution. Streamlines are colored by relative velocity magnitude and drawn in the relative frame of reference. The leakage vortex impinges on the neighbouring blade and creates local loss region. This lossy region moves towards the mid-span as clearance increased. The magnitude of the relative total pressure just at the downstream of the fan rotor with 1.71% tip clearance is shown in Figure 13. This Figure is drawn just downstream of the fan rotor and the visualization plane is aligned with the trailing edge of the rotor blade. Red regions in the Figure shows the highest total pressure regions while dark blue region shows lowest total pressure regions. The dark blue region near the fan rotor hub clearly shows the loss generation near endwall surface due to the combination of hub corner separation and three dimensional hub endwall flow. The

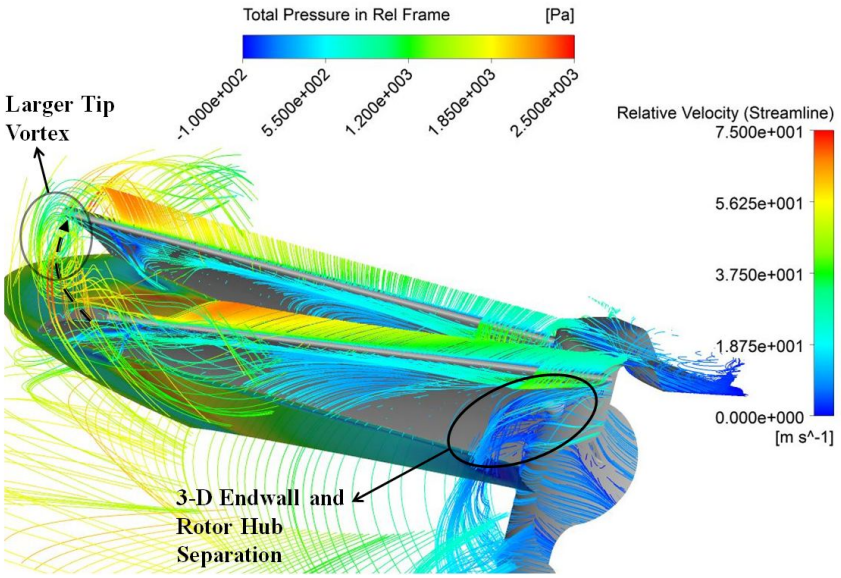

FIGURE 12: Streamlines around the baseline rotor blade with 1.71 % tip clearance and rotor hub at 2400 rpm

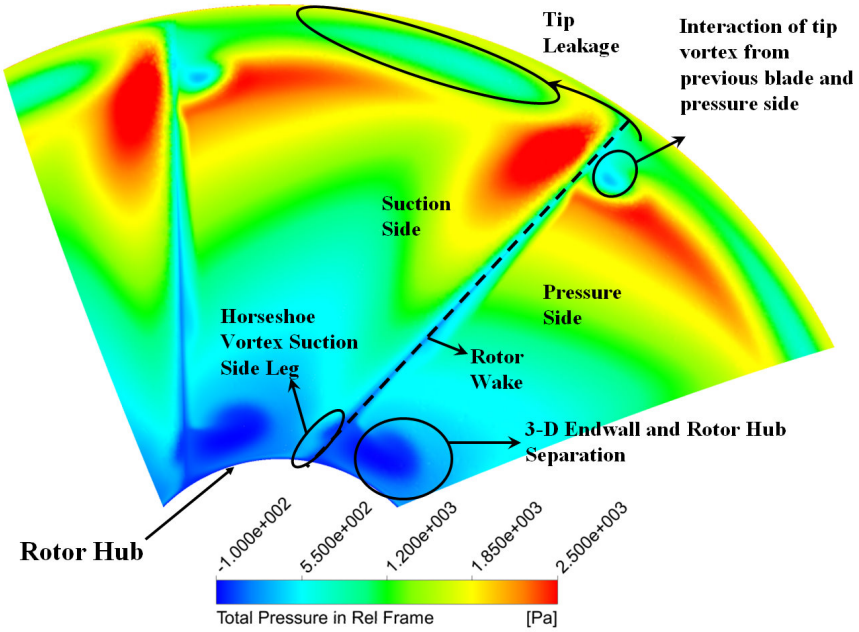

FIGURE 13: Relative total pressure distribution at the rotor exit plane for the baseline blade with 1.71 % tip clearance

wake region of the rotor blade is shown with dashed lines in Figure 13. The tip leakage flow and tip vortex is also visible near the rotor tip. The light blue region near the rotor tip shows the blokage effect that is induced by tip vortex originating from the rotor blade pressure side. There is also another light blue region near the pressure side of the rotor blade. That shows interaction of the tip vortex propagating from the previous rotor blade with the pressure side as shown in Figure 13. This interaction can also be seen in Figure 12 by the streamlines drawn around the rotor tip. This interaction near the pressure side results in a measurable total pressure drop at the exit of the fan blade because of separation from the pressure side.

Figure 15 shows the effect of tip clearance and other important 3D passage flow features on the rotor exit relative total pres-

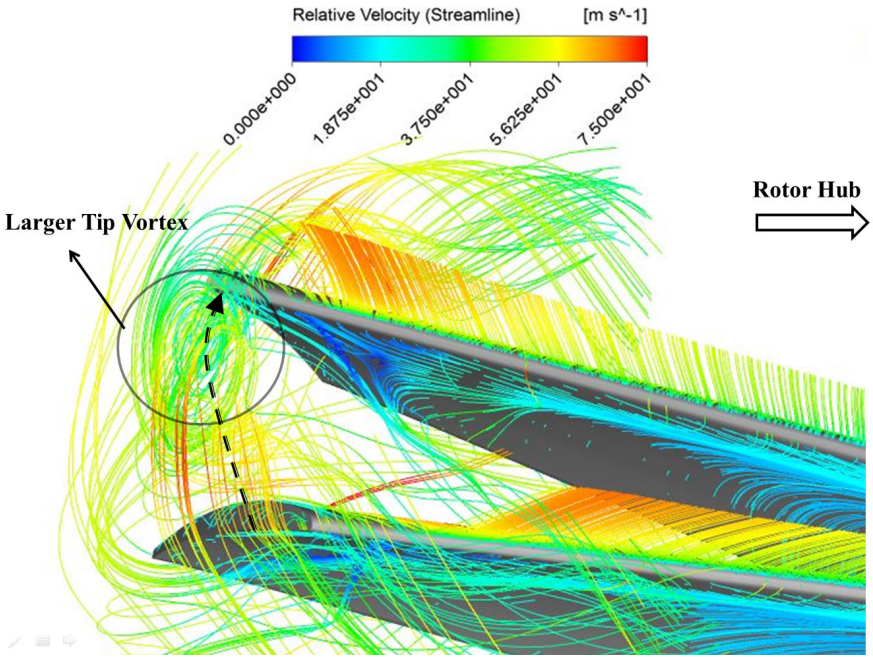

FIGURE 14: Streamlines around the baseline rotor blade with 3.04 % tip clearance and rotor hub at 2400 rpm

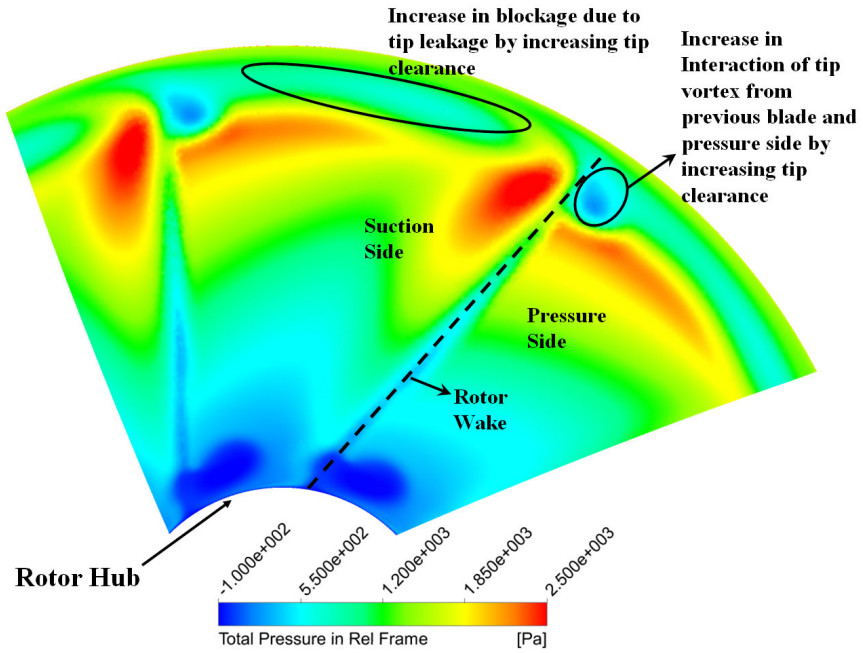

FIGURE 15: Relative total pressure distribution at the rotor exit plane for the baseline blade with 3.04 % tip clearance

sure distribution for a tip clearance value of 3.04%. This Figure is drawn at the same plane that is used in Figure 13 Changing the clearance level didn't affect this distribution near the hub region. However, an increase in tip clearance resulted in more aerodynamic loss near the rotor tip. Overall blockage due to tip leakage is also increased. Besides, the interaction of tip vortex and rotor blade pressure side is much enhanced and more total pressure loss is obviously generated in the passage. Figure 16 shows

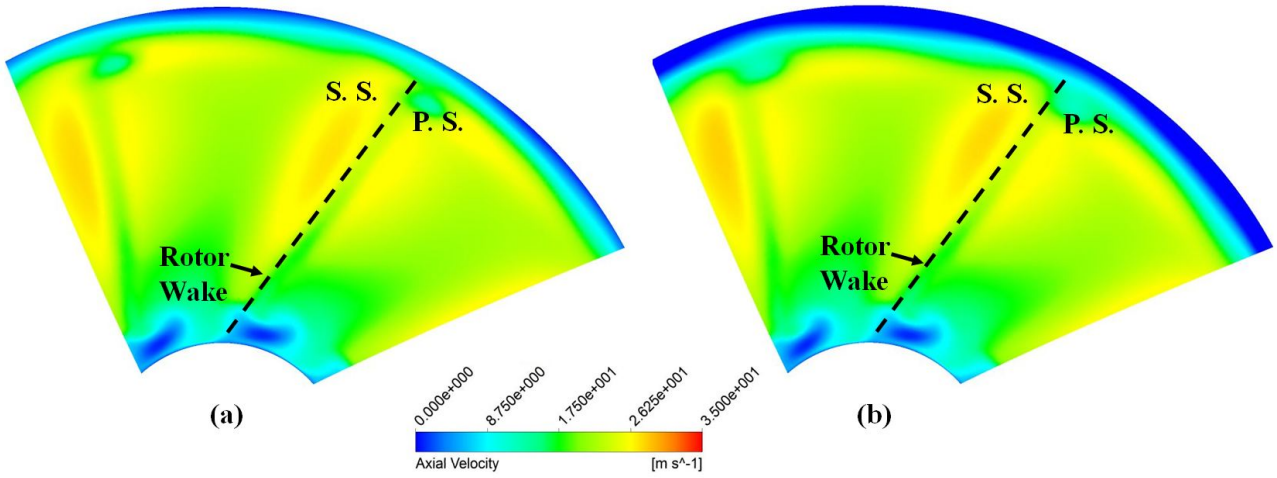

FIGURE 16: Axial velocity comparison at the rotor exit plane for baseline blade with (a) 1.71% and (b) 3.04% tip clearance

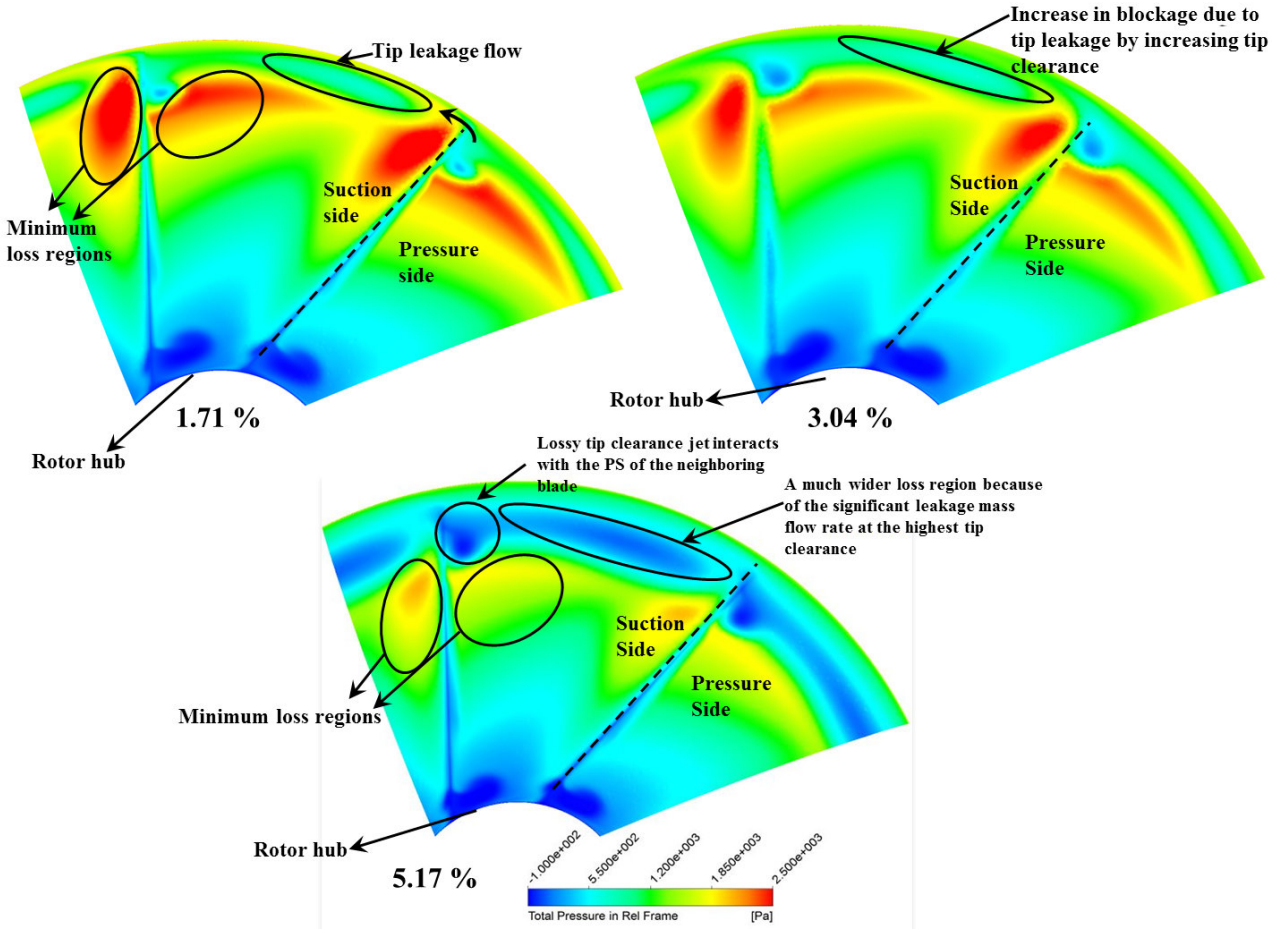

FIGURE 17: Relative total pressure comparison at the rotor exit plane for the baseline blades with 1.71%,3.04% and 5.17% tip clearance

the comparison of axial velocity at the downstream of the fan rotor. The low momentum fluid near hub region is shown by dark blue color. This region wasn't affected from changing the tip clearance level. The tip leakage losses were increased by increasing the tip clearance. An increase in the size of the blockage due to tip vortex is observed by comparing the dark blue regions near the casing for 1.71 % and 3.04 %tip clearances. The size of the dark blue area increased for the 3.04 % tip clearance.

The effect of increasing tip clearance is shown in Figure 17. Three different tip clearances were compared by total pressure contours drawn at the downstream of the fan rotor, and the visualization plane is aligned with the trailing edge of the rotor blade. When tip clearance was increased to 5.17 %, tip leakage losses were increased tremendously due to stronger tip clearance jet. This lossy leakage flow interacts with the pressure side of the neighbouring blade. This impinging leakage jet creates a relatively large local loss region and moves towards the mid span. A much wider total pressure loss region was created because of the significant leakage mass flow rate at the highest tip clearance. The minimum loss regions indicated by red are shrinking as shown by orange and yellow zones for the 5.17%.

CONCLUSIONS

Experimental investigations and computational analyses were performed for the development of novel tip geometries that are applicable to ducted fans used in VTOL UAV systems. The computational method that will be a major design analysis tool for the design of novel tip geometries is validated via experimental data presented throughout this paper.

A 22" diameter ducted fan test system was designed and manufactured for experimental investigations of tip leakage flow in ducted fans. Fan rotor exit total pressure surveys and duct inlet total pressure and velocity measurements were carried out for aerodynamic performance quantifications. A six component force and torque transducer was used for aeromechanic performance quantification.

A high resolution simulation of the flow field around the rotating fan rotor blades was performed by solving Reynolds Averaged Navier Stokes equations using a general purpose solver Ansys-CFX. The computational analysis was extensively used in designing the tip treatments.

When 3.04 % clearance results are compared to the rotor only result, up to 38% increase in ducted fan hover efficiency can be obtained at higher rotor speeds. That increase is mainly the result of using duct around an open rotor.

A steady-state RANS simulation of fan rotor blades and duct geometry showed very good agreement with the measured total pressure distribution especially near the tip region of the rotor in the 22" diameter ducted fan research facility.

Experimental investigations of baseline rotor showed that decreasing tip clearance increased the thrust obtained from the ducted fan in hover condition. Decreasing the tip clearance from 3.04 % to 1.71 % also increased hover efficieny of the system by 17.85 % at higher rotor speeds.

When the tip clearance increased from 3.04 % to 5.17 %, Up to 18.1 % drop in hover efficiency was observed .

Since the agreement between the experimental results obtained from the 22 inch diameter ducted fan and the 3D RANS based computations is very good, the present computational tool forms a strong design/analysis basis for future tip treatments that can be developed by computational means.

The results from an investigation dealing with the new tip treatments designed and analyzed using this validated computational approach are presented in an accompanying paper by Akturk and Camci [17].

ACKNOWLEDGMENT

The authors acknowledge the financial support provided by the PSU Vertical Lift Center of Excellence (VLRCOE)and National Rotorcraft Technology Center (NRTC) (Under U.S. Army Research Office grant # W911W6-06-2-0008). They wish to thank to Ozhan Turgut for his support throughout this effort. They are also indebted to Mr. Harry Houtz for his technical support.

REFERENCES

[1] Lee, G. H., Baek, J. H., and Myung, H. J., 2003. "Structure of tip leakage in a forward-swept axial-flow fan". *Flow, Turbulence and Combustion,* ***70***, pp. 241–265.

[2] Jang, C. M., Furukawa, M., and Inoue, M., 2001. "Analysis of vortical flow field in a propeller fan by ldv measurements and les - parts i, ii". *Journal of Fluids Engineering,* ***123***, pp. 748–761.

[3] Storer, J. A., and Cumpsty, N. A., 1991. "Tip leakage flow in axial compressors". *Journal of Turbomachinery,* ***113***, April.

[4] Lakshminarayana, B., Zaccaria, M., and Marathe, B., 1995. "The structure of tip clearance flow in axial flow compressors". *Journal of Turbomachinery,* ***117***, pp. 336–347.

[5] Matzgeller, R., Bur, P., and Kawall, J., 2010. "Investigation of compressor tip clearance flow structure". *Proceedings of ASME Turbo Expo 2010:Power for Land, Sea and Air,* ***GT2010-23244***.

[6] Inoue, M., Kuroumaru, M., and Furukawa, M., 1986. "Behavior of tip leakage flow behind an axial compressor rotor". *Journal of Gas Turbine and Power,* ***108***, pp. 7–14.

[7] Furukawa, M., Inoue, M., Kuroumaru, M., Saik, i. K., and Yamada, K., 1999. "The role of tip leakage vortex breakdown in compressor rotor aerodynamics". *Journal of Turbomachinery,* ***121***, pp. 469–480.

[8] Fujita, H., and Takata, H., 1984. "A study on configurations

of casing treatment for axial flow compressors". *Bulletin of the JSME,* ***27***, pp. 1675–1681.

[9] Moore, R. D., Kovich, G., and Blade, R. J., 1971. Effect of casing treatment on overall and blade-element performance of a compressor rotor. Tech. Rep. TN-D6538, NASA.

[10] Reynolds, B., Lakshminarayana, B., and Ravindranath, A., 1979. "Characteristics of near wake of a fan rotor blade". *AIAA Journal,* ***17***, pp. 959–967.

[11] Ravindranath, A., and Lakshminarayana, B., 1980. "Mean velocity and decay characteristics of near and far-wake of a compressor rotor blade of moderate loading". *Journal of Engineering for Power,* ***102***, pp. 535–547.

[12] Myung, H. J., and Baek, J. H., 1999. "Mean velocity characteristics behind a forward- swept axial-flow fan". *JSME Int. J.,* ***42***, pp. 476–488.

[13] Williams, R., Ingram, G., and Gregory-Smith, D., 2010. "Large tip clearance flows in two compressor cascades". *Proceedings of ASME Turbo Expo 2010:Power for Land, Sea and Air,* ***GT2010-22952***.

[14] Pereira, J. L., 2008. "Hover and wind-tunnel testing of shrouded rotors for improved micro air vehicle design". PhD thesis, University of Maryland, Maryland.

[15] Martin, P., and Tung, C., 2004. "Performance and flowfield measurements on a 10-inch ducted rotor vtol uav". *60th Annual Forum of the American Helicopter Society*.

[16] Martin, P. B., and Boxwell, D. A., 2005. "Design, analysis and experiments on a 10-inch ducted rotor vtol uav". *AHS International Specialists Meeting on Unmanned Rotorcraft: Design, Control and Testing*.

[17] Akturk, A., and Camci, C., 2011. "Tip clearance investigation of a ducted fan used in vtol uavs part 1: Novel treatments via computational design and their experimental verification". *Proceedings of ASME Turbo Expo 2011:Power for Land, Sea and Air,* ***GT2011-46359***.

[18] Corp, U. S. United sensors corporation kiel probe: general information. http://www. unitedsensorcorp.com/kiel.html.

[19] Wilcox, D. C., 1993. *Turbulence modeling for CFD*. La Caada: DCW Industries, Canada.

[20] Abemethy, R. B., Benedict, R. P., and B., D. R., 1985. "Asme measurement uncertainty". *ASME Journal of Fluids Engineering*.

[21] Abemethy, R. B., and B., R., 1985. "The history and statistical development of the new asme-sae-aiaa-iso measurement uncertainty methodology". *AIAA/SAE/ASME/ASEE 21st Joint Propulsion Conference & Exhibit*.